Conformal dual-band textile antenna with metasurface for WBAN application

Fatin Nabilah Giman[1] · Ping Jack Soh[1] ⓘ · Mohd Faizal Jamlos[1,2] ·
Herwansyah Lago[1] · Azremi Abdullah Al-Hadi[1] · Mohamedfareq Abdulmalek[3] ·
Nidhal Abdulaziz[3]

Abstract This paper presents the design of a dual-band wearable planar slotted dipole integrated with a metasurface. It operates in the 2.45 GHz (lower) and 5.8 GHz (upper) bands and made fully using textiles to suit wireless body area network applications. The metasurface in the form of an artificial magnetic conductor (AMC) plane is formed using a rectangular patch incorporated with a diamond-shaped slot to generate dual-phase response. This plane is then integrated with the planar slotted dipole antenna prior to its assessment in free space and bent configurations. Simulations and measurements indicated a good agreement, and the antenna featured an impedance bandwidth of 164 and 592 MHz in the lower and upper band, respectively. The presence of the AMC plane also minimized the backward radiation toward the human body and enhanced realized gains by up to 3.01 and 7.04 dB in the lower and upper band.

1 Introduction

Wearable devices and wireless body area networks (WBAN) are envisioned to change the landscapes of body-worn sensors, medicine, health monitoring, and emergency rescue [1–9]. Enabling seamless accessibility between the 2.4 GHz WBAN frequency and the widely used Industrial, Scientific, and Medical (ISM; 5.2 GHz) band [2] requires WBAN devices to be capable of operating in both frequencies using a single hardware. Besides that, a wearable system is envisioned to be conformal, lightweight, miniature in size, low profile, inexpensive, and easy to fabricate to ensure its attractiveness. In recent years, textile antenna has been widely investigated as the main enabling technology for wearable devices. The choice of such material is mainly due to its ease of integration on clothing. Any fabric such as felt [1–5], silk, tween, panama, moleskin, fleece, PTFE, Perspex [5], denim jeans [6–8], nylon [9], etc., are potentially suitable as its substrate. Meanwhile, e-textiles are generally used to form its conducting elements and are required to be low in resistivity and flexible. They should preferably not be elastic due to the proneness of such antennas to easily degrade when deformed (stretched or bent). Meanwhile, metasurfaces such as artificial magnetic conductor (AMC), high impedance surface (HIS), and electromagnetic bandgap (EBG) structures are widely used due to its compatibility with low profile antennas. They can also be located close to the radiating elements and operate as their reflectors to reduce backward radiation of the overall structure toward the human body [1–5, 10–15]. One of the main advantages of AMC is its simple unit cell basic structure, which are typically square or rectangular-shaped patches. Besides that, such AMC is capable of operating across the 5 GHz wireless local area network (WLAN) band due to its wide bandwidth when properly optimized. In this paper, a dual-band planar textile slotted dipole integrated with an AMC plane operating in the WBAN and WLAN bands (2.45 and 5.8 GHz) is presented. Besides in planar condition, its operation has been studied under two different bending

✉ Ping Jack Soh
  pjsoh@unimap.edu.my

[1] Advanced Communication Enginerring Centre (ACE),
    School of Computer and Communication Engineering,
    Universiti Malaysia Perlis (UniMAP), Pauh Putra,
    02600 Arau, Perlis, Malaysia

[2] Faculty of Mechanical Engineering, Universiti Malaysia
    Pahang, Pekan, Malaysia

[3] Faculty of Engineering and Information Sciences, University
    of Wollongong in Dubai, Dubai Knowledge Village Dubai,
    United Arab Emirates

directions (*x*-axis and *y*-axis) around the human upper arm of different radii. Besides bending, specific absorption rate (SAR) is also assessed to evaluate the safety level of antenna operation in the vicinity of the human body based on [16].

2 Antenna and material specification

2.1 Characterization of the metasurface

The AMC is designed on a felt substrate with a thickness of 3 mm, relative permittivity (ε_r) of 1.44, and loss tangent (tan-δ) of 0.044. Its conductive elements are formed using a 0.17-mm-thick ShieldIt Super with an estimated conductivity of 1.18×10^5 S/m. The AMC topology is illustrated in Fig. 1. Its unit cell structure is formed using five layers consisting of two 3-mm-thick substrate layers and three layers of ShieldIt. A full ground plane occupies the bottom-most layer, while the proposed AMC plane is located in between the two substrate layers. The dipole described in the following sections is planned to be placed on the top layer. The AMC plane is formed using a 3 × 3 array of rectangular patch, each integrated with a diamond-shaped slot as illustrated in Fig. 1b, c. The size of the inner and outer diamond-shaped slot determines the reflection phase points of the dual-band AMC. The shorter current path provided by the diamond-shaped slot resulted in a reflection phase bandwidth of 831 MHz (from 5.26 to 6.1 GHz) in the upper band. Meanwhile, the rectangular patch with a longer electrical length created a reflection phase bandwidth of 227 MHz (from 2.38 to 2.61 GHz) in the lower band. Its performance in both bands is illustrated in Fig. 1d.

2.2 Antenna design

The proposed dual-band planar slotted dipole antenna is shown in Fig. 2. It is designed based on the conventional dipole topology [1] for operation in the 2.45 GHz (lower) and 5.8 GHz (upper) bands. It combines a slot antenna (planar magnetic dipole) with an electric dipole. Next, four slots in the *x*-direction are introduced onto rectangular patch to enable its dual-band characteristics. Careful selection of their sizes will enable proper resonance at the desired lower and upper bands. The overall dimension of the proposed antenna is 90 mm × 90 mm. It is built using the same felt and ShieldIt textiles and is placed over the AMC plane.

(a)

(b)   **(c)**

(d)
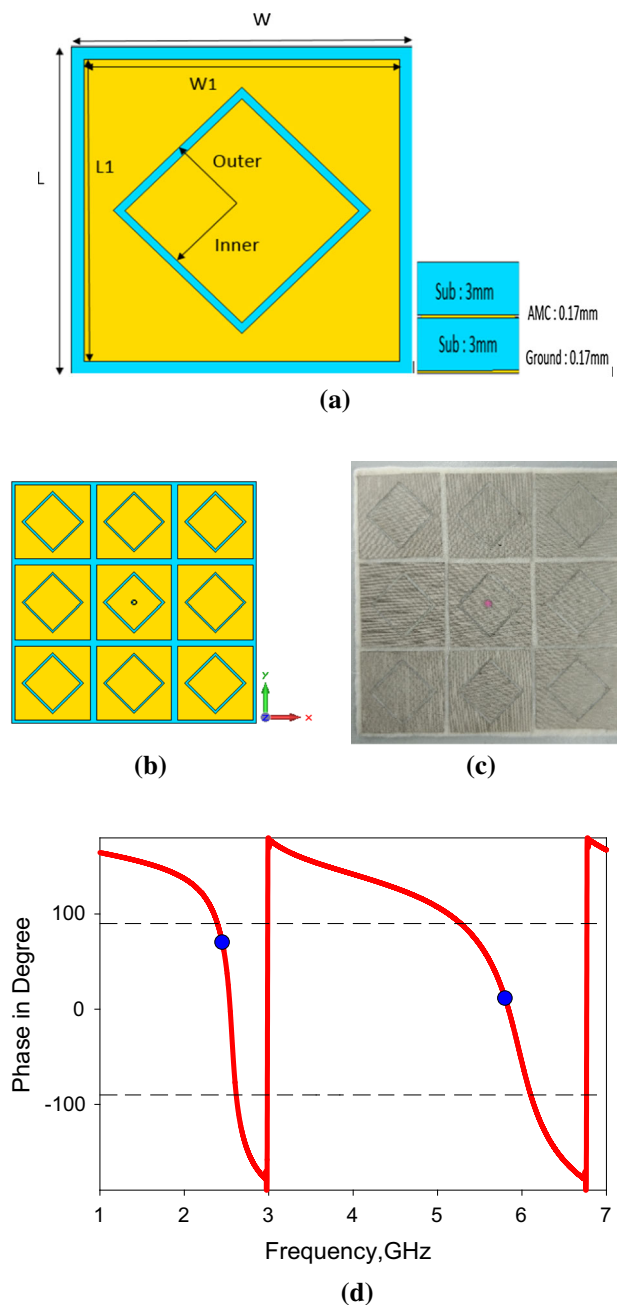
Fig. 1 **a** Unit cell of the dual-band AMC; **b** the 3 × 3 AMC plane; **c** fabricated AMC plane; and **d** reflection phase of proposed AMC. The dimensions of AMC unit cell (in mm) are $L = 30$, $W = 30$, $L1 = 27.75$, $W1 = 27.75$, inner $= 10.3$, outer $= 11.3$

3 Results and discussions

Besides studying its performance in free space, the antenna performance is analyzed in bent conditions as it is expected that the on-body placement will result in some degree of

**(a)**   **(b)**

(c)

(d)
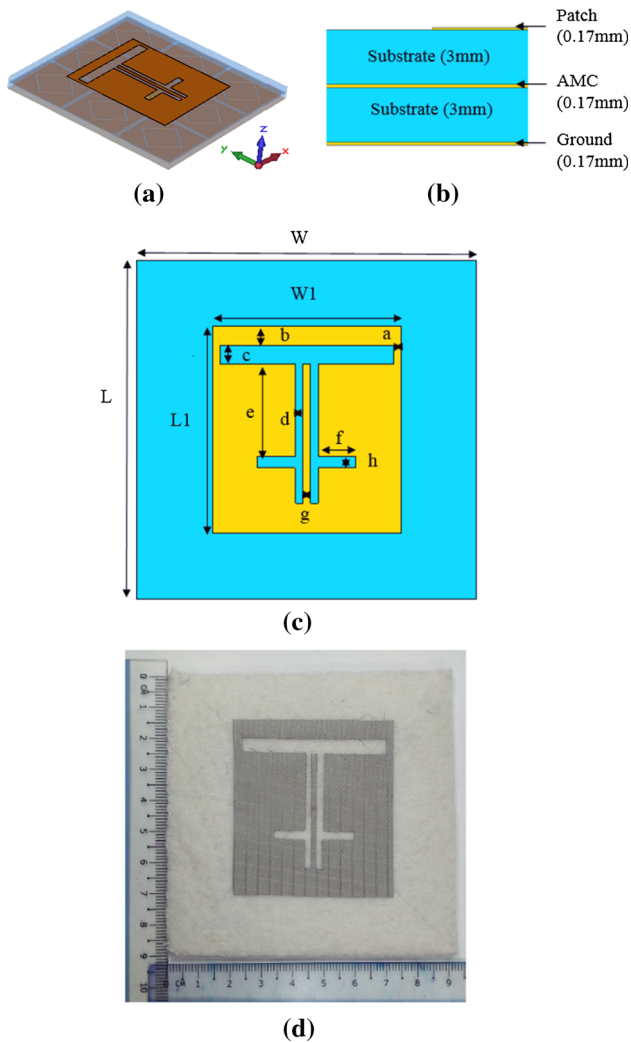
Fig. 2 Details of the proposed antenna: **a** 3D view, **b** cross section; **c** topology; and **d** fabricated antenna. The dimensions of the proposed antenna (in mm) are $L = 90$, $W = 90$, $L1 = 55$, $W1 = 50$, $a = 2$, $b = 5$, $c = 5$, $d = 2$, $e = 37$, $f = 10$, $g = 1$, $h = 3$

deformation. In this work, the antenna is studied in the planar and two other bending conditions using CST Microwave Studio (MWS). Their performance is compared in the following sub-sections.

3.1 Planar antenna

The antenna in the planar state initially provided an impedance bandwidth of 162 and 592 MHz in the 2.45 and 5.8 GHz bands, respectively, see Fig. 3.

The reflection coefficient (S_{11}) is -12.97 dB at 2.45 GHz and -24.95 dB at 5.8 GHz. The planar antenna produced a directional radiation pattern and reduced back-lobe radiation. This is important as omnidirectional antenna usually results in a relatively higher SAR in the human body, potentially affecting the health of body tissues [3]. The simulated front-to-back ratio (FBR) is higher
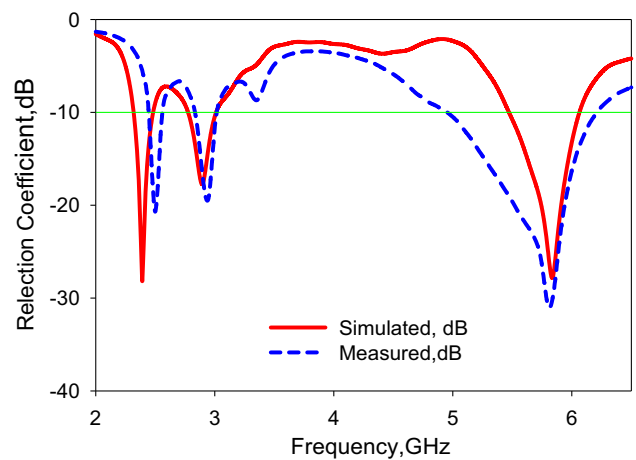

Fig. 3 Simulated and measured reflection coefficient of the proposed antenna (in planar condition) in free space

than 20 dB in the lower band and 32 dB in the upper band (Fig. 4). The realized gain of the antenna is about 3.01 dB at 2.45 GHz and 7.04 dB at 5.8 GHz.

3.2 Bending evaluations

To evaluate bending, the antenna is bent over cylindrical radii of $r = 40$ mm and $r = 60$ mm in the x-axis and y-axis, as illustrated in Fig. 5. The resulting S_{11} is shown in

(a)   **(b)**

(c)   **(d)**
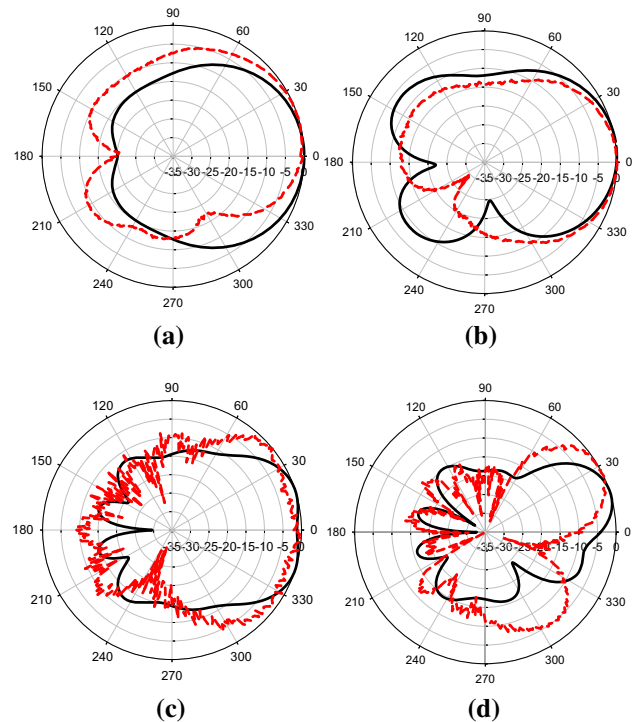
Fig. 4 Radiation patterns of the proposed antenna (in planar condition) in free space at; **a** 2.45 GHz (xz-plane); **b** 2.45 GHz (yz-plane); **c** 5.8 GHz (xz-plane); and **d** 5.8 GHz (yz-plane). Legend: Simulated (*black* solid line) and measured (*red* dashed line)
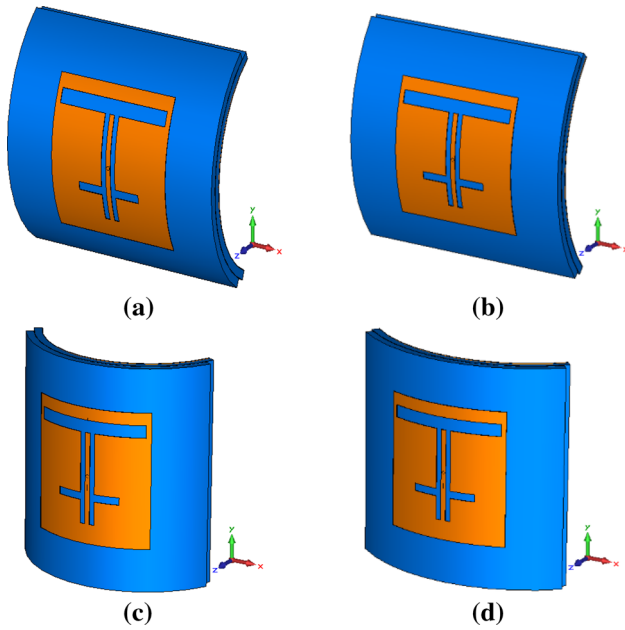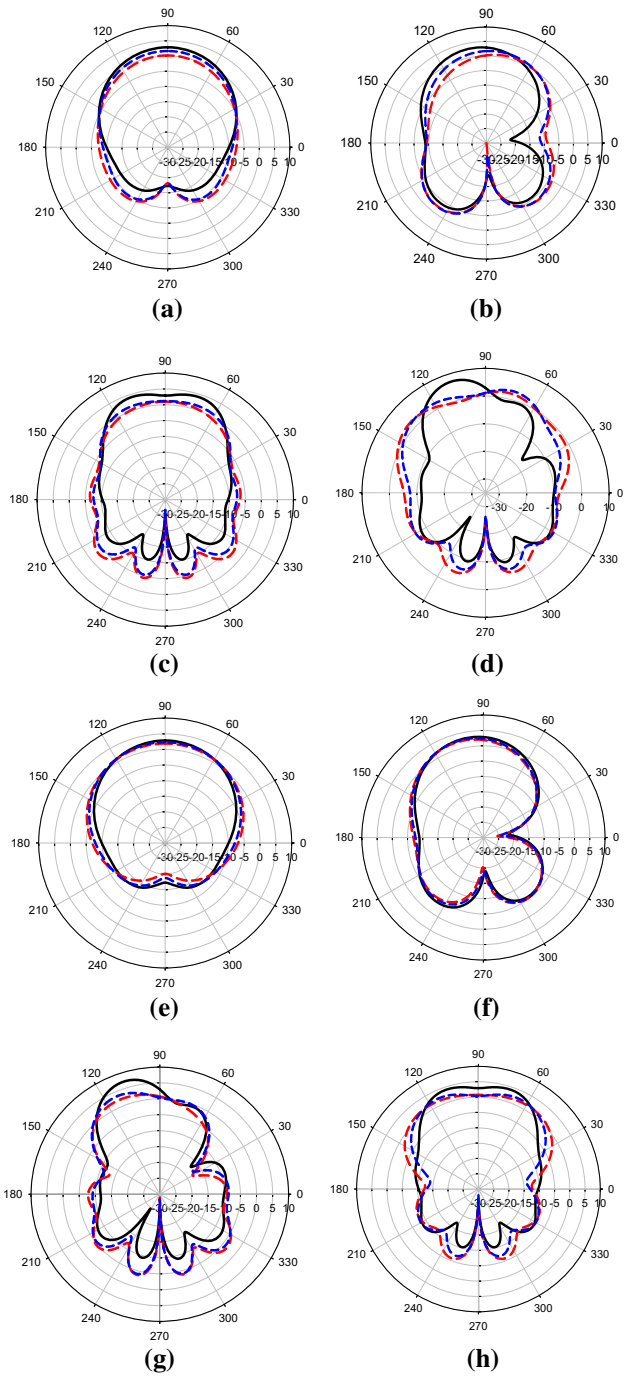
Fig. 5 Bending configuration of the proposed antenna: **a** at *x*-axis with *r* = 40 mm; **b** at *x*-axis with *r* = 60 mm; **c** at *y*-axis with *r* = 40 mm; and **d** at *y*-axis with *r* = 60 mm
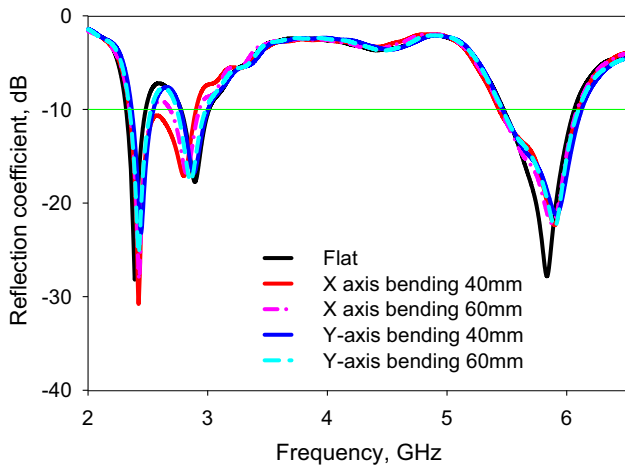
Fig. 6 Simulated reflection coefficient comparison of flat and bent antennas

Fig. 7 Simulated radiation patterns for the planar and bent antennas: **a** bent at the *x*-axis at 2.45 GHz (*xz*-plane); **b** bent at the *x*-axis at 2.45 GHz (*yz*-plane); **c** bent at the *x*-axis at 5.8 GHz (*xz*-plane); **d** bent at the *x*-axis at 5.8 GHz (*yz*-plane); **e** bent at the *y*-axis at 2.45 GHz (*xz*-plane); **f** bent at the *y*-axis at 2.45 GHz (*yz*-plane); **g** bent at the *y*-axis at 5.8 GHz (*xz*-plane); and **h** bent at the *y*-axis at 5.8 GHz (*yz*-plane). Legend: solid (*black*) line: planar antenna; (*red*) long dash line: bent with *r* = 40 mm; (*blue*) short dash line: bent with *r* = 60 mm

Fig. 6. It can be observed when the bending radius is reduced; the bandwidth in the lower band increases, while the upper bandwidth narrows with bending at both *x*- and *y*-axes. The antenna S_{11} improved by about 3 dB at 2.45 GHz when bent in the *x*-axis with *r* = 40 mm. On the contrary, similar S_{11} values with small degradations are observed at both frequencies when bent in the *y*-axis. Nonetheless, the operation of the antenna in the desired bands is maintained with $S_{11} < -10$ dB.

Figure 7 shows the radiation pattern comparison of the proposed antenna at 2.45 and 5.8 GHz in the planar form (in the *xz*- and *yz*-planes) and when bent (at the *x*- and

y-axes). It can be seen that the bending did not severely affect the directional antenna pattern and therefore can be efficiently used in wearable applications. It also maintained

**Table 1** Performance comparison of the proposed antenna in the planar and different bending configurations

Parameter	Condition of antenna	Frequency (GHz)	
		2.45	5.8
Reflection coefficient (dB)	Flat	−12.97	−24.95
	Bent at x-axis; r = 40 mm	−16.24	−19.08
	Bent at x-axis; r = 60 mm	−16.27	−20.33
	Bent at y-axis; r = 40 mm	−12.73	−19.73
	Bent at y-axis; r = 60 mm	−12.78	−19.81
Realized Gain (dB)	Flat	3.01	7.04
	Bent at x-axis; r = 40 mm	0.75	2.38
	Bent at x-axis; r = 60 mm	1.7	3.34
	Bent at y-axis; r = 40 mm	2.34	4.24
	Bent at y-axis; r = 60 mm	2.66	4.25
Directivity (dBi)	Flat	7.72	11.4
	Bent at x-axis; r = 40 mm	5.59	6.34
	Bent at x-axis; r = 60 mm	6.28	7.38
	Bent at y-axis; r = 40 mm	6.68	8.29
	Bent at y-axis; r = 60 mm	7.07	8.52
Bandwidth (MHz)	Flat	164	592
	Bent at x-axis; r = 40 mm	560	666
	Bent at x-axis; r = 60 mm	198	641
	Bent at y-axis; r = 40 mm	182	661
	Bent at y-axis; r = 60 mm	181	637
Front-to-back ratio (FBR (dB))	Flat	20.32	32.69
	Bent at x-axis; r = 40 mm	18.94	27.5
	Bent at x-axis; r = 60 mm	19.81	29.78
	Bent at y-axis; r = 40 mm	22.48	27.99
	Bent at y-axis; r = 60 mm	21.44	31.77

a directional pattern with high FBR, which implies reduced backward radiation.

Contrary to expectations, it is also seen that the bent antenna (for $r = 40$ and 60 mm) at x-axis provided the most significant improvement in terms of impedance bandwidth. An impedance bandwidth of 560 MHz (when bent with $r = 40$ mm) and 198 MHz (with $r = 60$ mm) is featured in the lower and upper band, respectively. In contrast, only 164 MHz (in the planar condition) of bandwidth is featured in the lower and upper bands, respectively. In general, the performance of the proposed antenna is satisfactory in terms of reflection coefficient, realized gain, directivity, bandwidth, and FBR in the flat and both bent conditions at 2.45 and 5.8 GHz. The performance of the proposed antenna is summarized in Table 1.

3.3 Specific absorption rate (SAR) analysis

To analyze the contribution of the proposed metasurface on the antenna, a series of SAR simulation is performed when it is bent around the upper arm of a Hugo human body model. The antenna is located 10 mm from this model
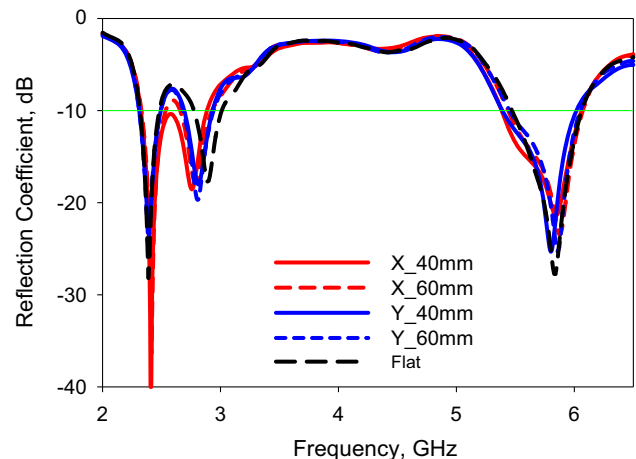

Fig. 8 Simulated reflection coefficient of the proposed antenna with varying bending conditions

considering both bending in the x-axis and y-axis. Figure 8 compares the simulated reflection coefficient of the proposed antenna with a varying degree of bending in the azimuth and elevation planes (with different radii). The

Table 2 Simulated SAR of the proposed antenna under different bending configurations

Frequency (GHz)	Condition of antenna	SAR (W/Kg)
2.45	Bent at x-axis; $r = 40$ mm	0.2
	Bent at x-axis; $r = 60$ mm	0.15
	Bent at y-axis; $r = 40$ mm	0.14
	Bent at y-axis; $r = 60$ mm	0.088
5.8	Bent at x-axis; $r = 40$ mm	0.165
	Bent at x-axis; $r = 60$ mm	0.97
	Bent at y-axis; $r = 40$ mm	0.11
	Bent at y-axis; $r = 60$ mm	0.054
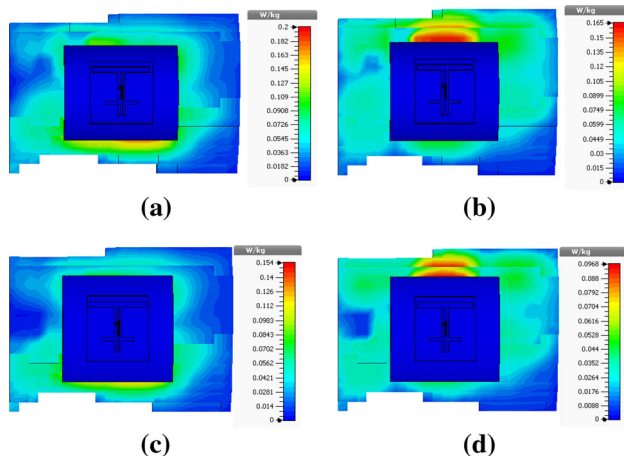
Fig. 9 SAR distribution of antenna bent at the x-axis with: **a** $r = 40$ mm at 2.45 GHz; **b** $r = 40$ mm at 5.8 GHz; **c** $r = 60$ mm at 2.45 GHz; and **d** $r = 60$ mm at 5.8 GHz

calculated SAR values are summarized in Table 2. It is observed that the SAR value decreased with increasing frequency at both bending directions. However, when bending 60 mm at the x-axis, an increasing SAR value is evident with the increase in frequency. Nonetheless, all assessed SAR are acceptable since they do not exceed 2 W/kg averaged over 10 g of tissue, based on the European regulatory requirements (Figs. 9, 10).

4 Conclusions

A wearable dual-band antenna with dual-band AMC is proposed for operation in the 2.4 and 5.8 GHz frequency bands for WBAN/WLAN applications. The antenna features a directional radiation and high FBR which potentially reduces SAR. The AMC plane is integrated with the antenna to reduce back radiation toward the human body. It consists of a 3×3 array of rectangular patches slotted with diamond-shaped slots to enable dual-band operation. This AMC structure is then combined with a patch antenna
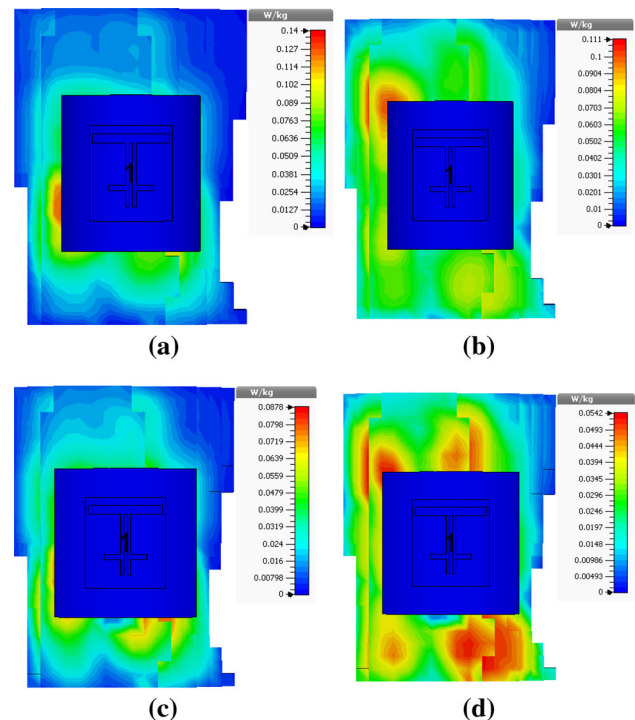
Fig. 10 SAR distribution of antenna bent at the y-axis with: **a** $r = 40$ mm at 2.45 GHz; **b** $r = 40$ mm at 5.8 GHz; **c** $r = 60$ mm at 2.45 GHz; and **d** $r = 60$ mm at 5.8 GHz

with a slotted dipole to enable its dual-band property. The performance of proposed antenna is satisfactory in terms of reflection coefficient, gain, directivity, radiation pattern, and bandwidth.

References

1. S. Yan, P.J. Soh, G.A.E. Vandenbosch, Low-profile dual-band textile antenna with artificial magnetic conductor plane. IEEE Trans. Antennas Propag. **62**(12), 6487–6490 (2014)
2. A. Afridi, S. Ullah, S. Khan, A. Ahmed, A.H. Khalil, M.A. Tarar, Design of dual band wearable antenna using metamaterials. J. Microw. Power Electromagn. Energy **47**(2), 126–137 (2013)
3. S. Yan, P.J. Soh, G.A.E. Vandenbosch, Wearable dual-band magneto-electric dipole antenna for WBAN/WLAN applications. IEEE Trans. Antennas Propag. **63**(9), 4165–4169 (2015)
4. S. Yan, P.J. Soh, G.A.E. Vandenbosch, Compact all-textile dual-band antenna loaded with metamaterial-inspired structure. IEEE Antennas Wirel. Propag. Lett. **14**, 1486–1489 (2015)
5. S. Zhu, R. Langley, Dual-band wearable textile antenna on an EBG substrate. IEEE Trans. Antennas Propag. **57**(4), 926–935 (2009)
6. M. A. Abdullah, M. K. A. Rahim, M. E. Jalil, N. A. Samsuri and N. A. Murad, Integrated two textile dipole antenna with dual-band textile artificial magnetic conductor. *7th European*

Conference on Antennas and Propag. (EuCAP), Gothenburg, Sweden, pp. 2075–2078, 8–12 Apr 2013

7. M. Grilo, and F. S. Correra, Parametric study of rectangular patch antenna using denim textile material. *SBMO/IEEE MTT-S International Microwave & Optoelectronics Conference (IMOC),* Rio de Janeiro, Brazil, pp. 1–5, 4–7 Aug 2013

8. S. K. Mishra, V. Mishra and N. Purohit, Design of wide band circularly polarized textile antenna for ISM bands at 2.4 and 5.8 GHz. *Signal Processing, Informatics, Communication and Energy Systems (SPICES),* pp. 1–5, 2015

9. D. L. Paul, M. Klemm, C. J. Railton and J. P. McGeehan, Textile Broadband E-Patch Antenna at ISM Band. *2007 IET Seminar on Antennas and Propag. for Body-Centric Wireless Communications,* London, pp. 38–43, 24 April 2007

10. M. N. Pavan and N. Chattoraj, Design and analysis of a frequency reconfigurable antenna using metasurface for wireless applications, in *2nd International Conference on Innovations in Information, Embedded and Communication systems (ICIIECS),* Coimbatore, pp. 1–5, 19–20 March 2015

11. Y. H. Di, X. Y. Liu and M. M. Tentzeris, A Conformable Dual-Band Antenna Equipped with AMC for WBAN Applications, in *3rd Asia-Pacific Conference on Antennas and Propag.(APCAP),* Harbin, China, pp. 388–391, 26–29 July 2014

12. Z.H. Jiang, D.E. Brocker, P.E. Sieber, D.H. Werner, A compact, low-profile metasurface-enabled antenna for wearable medical body-area network devices. IEEE Trans. Antennas Propag. **62**(8), 4021–4030 (2014)

13. R.C. Hadarig, M.E. de Cos, F. Las-Heras, Microstrip patch antenna bandwidth enhancement using AMC/EBG structures. Int. J. Antennas Propag. **12**, 1–7 (2012)

14. M. Cekingen, C. Isik and B. Turetken, Design of a broadband microstrip antenna with artificial magnetic conductor ground plane. *2011 7th International Conference on Electrical and Electronics Engineering (ELECO),* Bursa, Turkey, pp. 226–229, 1–4 Dec 2011

15. A. Foroozesh, L. Shafai, Effects of artificial magnetic conductors in the design of low-profile high-gain planar antennas with high-permittivity dielectric superstrate. IEEE Antennas Wirel. Propag. Lett. **8**, 1536 (2009)

16. P.J. Soh, G.A.E. Vandenbosch, F.H. Wee, A. van den Bosch, M. Martinez-Vazquez, D. Schreurs, Specific absorption rate (SAR) evaluation of textile antennas. IEEE Antennas Propag. Mag. **57**(2), 229–240 (2015)